Peptide Amphiphile Self-Assembly

DOI: 10.1002/anie.201201173

Remodeling Cross-β Nanotube Surfaces with Peptide/Lipid Chimeras**

Rong Ni, W. Seth Childers, Kenneth I. Hardcastle, Anil K. Mehta, and David G. Lynn**

Peptide/lipid chimeras, which are generally referred to as peptide amphiphiles, array specific peptides on the surface of ordered lipid assemblies.[1] These materials are being explored as tissue scaffolds, in drug delivery, as antimicrobrials, and for biomineralization applications.[2–6] However, the increasing realization that simple peptides with high cross-β fold propensity can achieve long-range ordered arrays comparable to lipid amphiphiles has now allowed for the creation of an entirely new architectural framework. This framework not only offers precisely controlled positioning of charges and hydrophobic patches along a robust nanotube surface, but also the systematic adjustment of that spacing in a manner that to this point has been unrealized in self-assembling materials.

Peptide amphiphiles can achieve remarkable long-range order within a range of topological lipid phases.[2–6] For example, the elongated worm-like micelles have been modeled as having alkane interiors with peptide surfaces,[4] a morphology that reflects the same structural tension between head group and alkane that molds phospholipid assemblies.[5] This structure suggests that various self-assembling peptide elements might be able to extend the standard amphiphile tensions into new frameworks, and focused our attention on the strong self-organizing potential of the cross-β fold.[3,5,7,8] The nucleating core sequence of the amyloid forming Aβ-peptide associated with Alzheimer's disease, Aβ(16-22), $K^{16}LVFFAE^{22}$-NH_2, which organizes into diverse cross-β assemblies,[9–13] was acylated through conventional solid-phase Fmoc chemistry at the N-terminus with straight-chain fatty acids ranging in length from two to sixteen carbon atoms. The products were purified by RP-HPLC, assembled under a range of conditions, and the resulting assemblies scored by electron microscopy (EM).

Of the series assembled under acidic conditions, C_2 (*N*-acetyl) through C_4 (*N*-butyryl) assemblies were morphologically indistinguishable (Supporting Information, Figure S1), and assigned as hollow tubes based on the previously characterized *N*-acetyl-Aβ(16-22) assemblies.[10] Intermediate acyl chain lengths, C_5 to C_{10}, assembled as ribbons, and longer lengths, C_{14} and C_{16}, formed fibers (Supporting Information, Figure S1). Most notably however, the C_{11} (*N*-undecanoyl), C_{12} (*N*-lauroyl), and C_{13} (*N*-tridecanoyl) Aβ(16-22) chimeras appeared as homogeneous tubes most similar to the *N*-acetyl assemblies, with the same distinct edges that arise from negative staining by uranyl acetate deposition inside and outside the tube cavity (Figure 1b).

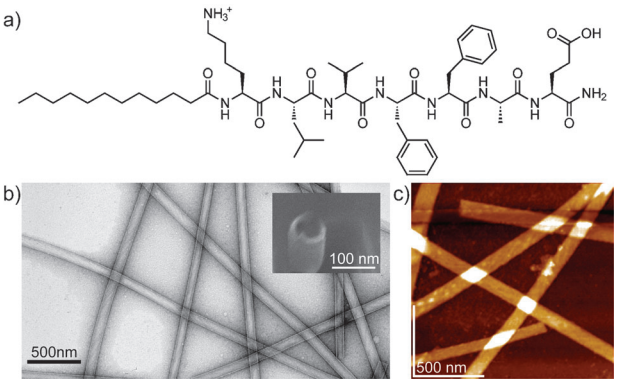

Figure 1. a) Structure of *N*-lauroyl-Aβ(16-22); b) TEM, cryo-SEM (inset), and c) AFM micrographs of 1.2 mM *N*-lauroyl-Aβ(16-22) assembled in 40% acetonitrile/water with 0.1% trifluoroacetic acid for 1–2 weeks.

High-resolution cryo-SEM further confirmed the *N*-lauroyl-Aβ(16–22) assemblies as hollow nanotubes (Figure 1b, inset) and the diameters of (56 ± 8) nm were also remarkably similar to the well-characterized *N*-acetyl-Aβ(16–22) tubes.[10] Powder X-ray diffraction analyses[14] (Figure 2a) gave sharp and distinct reflections for the H-bonded β-strand repeat at 4.7 Å for all acyl chain lengths, but the lamination (β-sheet stacking) reflection varied systematically from 9.8 Å for *N*-acetyl-Aβ(16–22) tubes to 11.5 Å for *N*-lauroyl-Aβ(16–22) tubes (Figure 2b), to multiple laminate *d* spacings of 9.8 Å and ≥ 13 Å for the C_{14} (*N*-myristoyl) and C_{16} (*N*-palmitoyl) assemblies, respectively. This ability to systematically control the laminate spacing by simply changing the length of the acyl chain offers an as yet inaccessible materials design element and it focused our attention on the complete characterization of the homogeneous *N*-lauroyl-Aβ(16-22) tubes.

Electron diffraction[13,15] (Figure 2c,d) and simulations[16] (Supporting Information, Figure S2) from the top and bottom walls of oriented tubes[10,17] defined a distinct tilt angle of the

[*] Dr. R. Ni, Dr. W. S. Childers, Dr. K. I. Hardcastle, Dr. A. K. Mehta, Prof. D. G. Lynn
Center for Fundamental and Applied Molecular Evolution, NSF/NASA Center for Chemical Evolution, and Departments of Chemistry and Biology, Emory University
Atlanta, GA 30322 (USA)
E-mail: anil.mehta@emory.edu
david.lynn@emory.edu

[**] We are indebted to Jeannette Taylor of the Robert P. Apkarian Microscopy Core, Emory University, for TEM, electron diffraction, and cryo-SEM training and collection. This work supported by the U.S. DOE (ER15377) and the NSF and NASA Astrobiology Program, under the NSF Center for Chemical Evolution, CHE-1004570.

Supporting information for this article is available on the WWW under http://dx.doi.org/10.1002/anie.201201173.

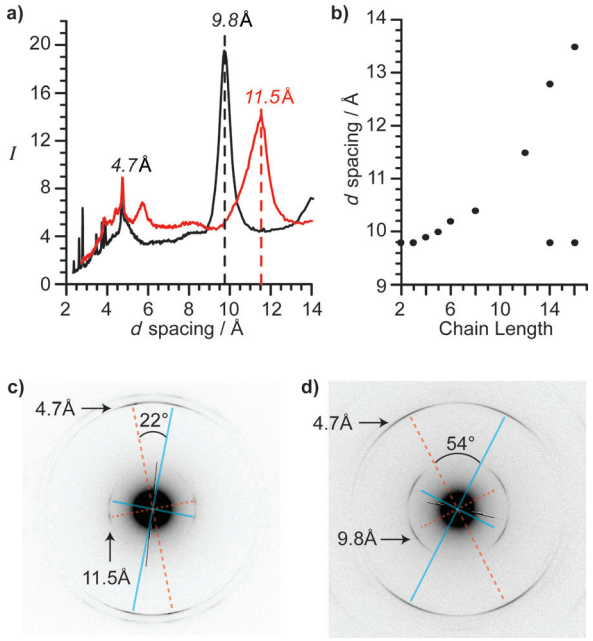

Figure 2. Powder and oriented electron diffraction of *N*-acyl-Aβ(16-22) peptide assemblies. a) X-ray powder diffraction of *N*-lauroyl-Aβ(16-22) (red) and *N*-acetyl-Aβ(16-22) tubes (black), indicating that each has a 4.7 Å H-bonding *d* spacing but differ in lamination *d* spacing (9.8 Å vs. 11.5 Å). b) Lamination spacing as a function of increasing N-terminal acyl chain length. c, d) Oriented electron diffraction of c) *N*-lauroyl-Aβ(16-22) tubes and d) *N*-acetyl-Aβ(16-22) tubes. The tube long axis is oriented vertically with respect to image. Each tube has two cross-β patterns, shown as solid blue and dashed red lines, owing to diffraction from the top and bottom tube walls.[10,17]

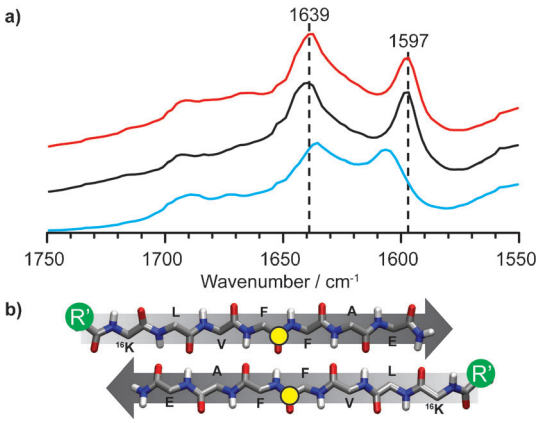

Figure 3. a) FTIR spectra of [1-^{13}C]Phe19 *N*-lauroyl-Aβ(16-22) tubes (red), *N*-acetyl Aβ(16-22) tubes (black), and *N*-acetyl Aβ(16-22) fibers (blue). The vertical dashed lines highlight the ^{12}C and ^{13}C stretches at 1639 cm^{-1} and 1597 cm^{-1} respectively, consistent with b) antiparallel one-residue out-of-register β-sheets.[10] *N*-Acetyl-Aβ(16-22) fibers assembled at neutral pH served as a control for antiparallel in-register β-sheets.[10] Yellow circles denote [1-^{13}C]Phe19 carbonyl carbon atoms and green circles indicate the position of acyl chain.

spiraling ribbon along the tube axis. The *N*-lauroyl-Aβ(16-22) tube tilt angle was 11°, which is less than half the 27° angle of the *N*-acetyl-Aβ(16-22) tubes.[10,17–18] This angle further implicates the laminate grove as the structural constraint most significantly impacted by addition of the *N*-lauroyl chain.

Indeed, the overall peptide architectures of the *N*-lauroyl and *N*-acetyl nanotubes were remarkably similar. Both tubes gave a wall thickness of 4 nm by atomic force microscopy (AFM) measurements (Figures 1c; Supporting Information, Figures S3 and S4), which is consistent with TEM and SEM analyses. Negatively charged gold colloidal particles bound to both assemblies with indistinguishable particle distribution and density (Supporting Information, Figure S5),[10,19] thus suggesting that the terminal lysine residues were protonated and equally accessible on each tube surface. Additionally, the amide I IR stretching modes at 1628 cm^{-1} (Supporting Information, Figure S6) and the common shoulder at 1693 cm^{-1} were observed for both tubes and are diagnostic of antiparallel strand arrangements.[20] Assemblies prepared with *N*-acetyl-[1-^{13}C]F19 Aβ(16-22) and *N*-lauroyl-[1-^{13}C]F19 Aβ(16-22) gave identical ^{12}C and ^{13}C band assignments at 1639 cm^{-1} and 1597 cm^{-1} (Figure 3),[12,21] uniquely aligning the Phe19 carbonyl groups and positioning the strands in a one-residue-out-of-register antiparallel configuration (Figure 3b).[10] Finally, when *N*-[1-^{13}C]lauroyl-Aβ(16-22) peptides assembled in the presence of 0.1% trifluoroacetic acid (TFA) were slowly bundled with Na_2SO_4/NADH and evaluated by solid-state NMR, ^{13}C{^{19}F}REDOR,[22] at least 50% of the ^{13}C signal was dephased by fluorine (Supporting Information, Figure S7), which is consistent with similar TFA access to the C_2 and C_{12} bilayer surfaces.[23]

These structural constraints placed the C_{12} acyl chain between the laminated β-sheets, but further constraints were required to position the acyl chain relative to the peptide backbone. We first attempted to localize the carbonyl end of the acyl chain by preparing and assembling *N*-[1-^{13}C]lauroyl-[^{15}N]L17 Aβ(16-22) for solid-state NMR analyses. The unbiased fit using a Boltzmann maximum-entropy approach (BS-REDOR)[24] of the ^{13}C{^{15}N}REDOR dephasing data as isolated ^{13}C–^{15}N spin pairs (Figure 4c,d) indicated that 92% of *N*-lauroyl carbonyl carbon atoms were 3.8 Å from the leucine amide backbone nitrogen atoms. A molecular mechanics conformational search of the assembly without distance constraints showed that the acyl chain could bend over the β-sheet sidechains and give a distance of (3.7 ± 0.3) Å from the lauroyl carbonyl carbon to the Leu17 nitrogen (Supporting Information, Figure S8). For reference, a fully extended chain (Figure 4a), analogous with the peptide amphiphile model, would have a lauroyl ^{13}CO to [^{15}N]Leu17 distance of 4.5 Å.

To constrain the remainder of the acyl chain, both *N*-[12-^{13}C]lauroyl-[^{15}N]V18 Aβ(16-22) and *N*-[12-^{13}C]lauroyl-[^{15}N]L17 Aβ(16-22) chimeras were prepared and assembled separately. The lauroyl ω-$^{13}CH_3$ ^{13}C{^{15}N}REDOR dephasing in the ^{15}N Val18 assemblies identified two distances (4.8 Å and 6 Å; Figure 5d). ^{13}C dephasing in the [^{15}N]Leu17 assemblies resolved as a single distance of 6.4 Å (Figure 5e); however at this distance, assuming that each ^{13}C is coupled to only a single ^{15}N, about 20% of the ω-CH_3 carbon atoms have dipolar couplings that are too weak to measure, even with 120 ms REDOR evolution times. The distance measurements on both ω-$^{13}CH_3$-enriched samples were consistent with the lauroyl chain methyl group being closer to the valine18

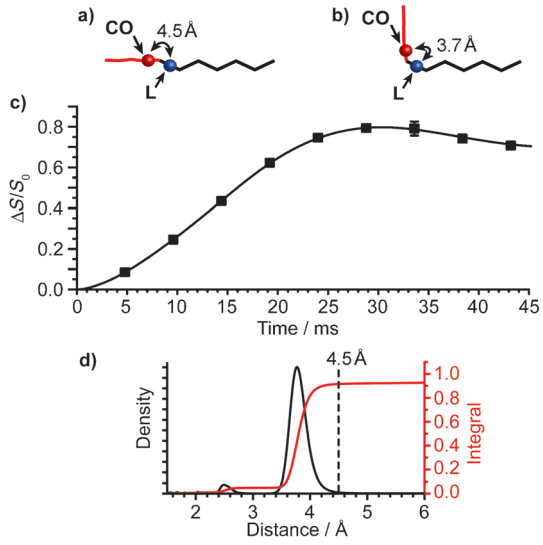

Figure 4. NMR ^{13}C–^{15}N distance measurements to localize acyl chain within cross-β laminate. a) Peptide amphiphile model with a fully extended and b) bent lauroyl chain. The peptide pleated backbone is shown as black lines, the position of the leucine nitrogen is shown as blue spheres, the lauroyl chain is drawn as a red line, and the lauroyl chain CO as red spheres. c) $^{13}C\{^{15}N\}$REDOR dephasing with calculated dephasing curve for distances from d) BS-REDOR fit, consistent with a ^{13}CO to [^{15}N]Leu distance centered at 3.7 Å.

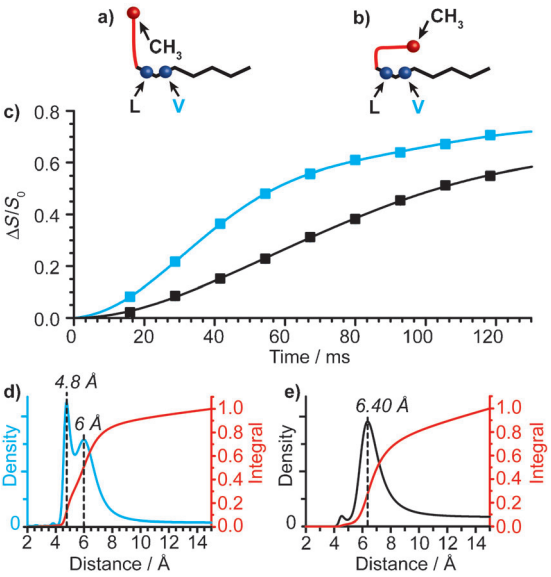

Figure 5. NMR ^{13}C–^{15}N distance measurements to distinguish between a) extended and b) bent lauroyl chain with CH_3 laying over peptide within cross-β laminate. The leucine (black) and valine (blue) nitrogen atoms and lauroyl methyl (red) are drawn as spheres. c) $^{13}C\{^{15}N\}$ REDOR measurement of *N*-[12-^{13}C]lauroyl-[^{15}N]L17 Aβ(16-22) (blue) and *N*-[12-^{13}C]lauroyl-[^{15}N]V18 Aβ(16-22) (black) peptide nanotubes. BS-REDOR fits (solid lines) with $^{13}CH_3$ to [^{15}N]Val distances centered at 4.8 Å (30%) and 6 Å (55%; blue), shown in (d), and with $^{13}CH_3$ to [^{15}N]Leu distances centered at 6.5 Å (80%; black), shown in (e).

nitrogen than the leucine17 nitrogen, and maps of the possible solutions for these NMR constraints place the ω-$^{13}CH_3$ well within the cross-β core (Figure 6a). Constraining both ends of

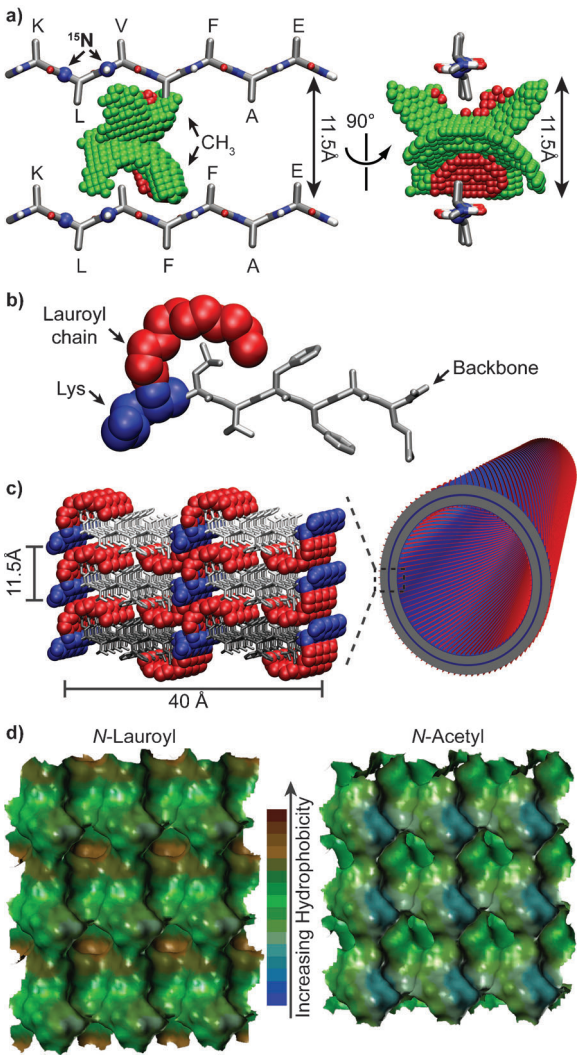

Figure 6. a) Allowable positions of the terminal $^{13}CH_3$ carbons for *N*-lauroyl-K[16] LVFFAE[22]-NH_2 that match the ^{13}C–^{15}N distances of 6.4 Å to [^{15}N]Leu and 4.8 Å to [^{15}N]Val (red spheres) or 6.4 Å to [^{15}N]Leu and 6 Å to [^{15}N]Val (green spheres). Blue spheres highlight leucine and valine nitrogen atoms. b) Model of lauroyl chain (red) packing within the β-strand. Lysine residue is colored blue; the peptide backbone and side chains are gray. c) Orientation and packing of *N*-lauroyl-KLVFFAE peptides within tube. Expansion shows three laminated β-sheets and a peptide–peptide bilayer, consistent with the structural data. d) Comparison of solvent-exposed surface patterns highlighting the lipophilic potential[26] for *N*-lauroyl and *N*-acetyl KLVFFAE tubes. The most hydrophobic (lipophilic) regions are colored brown and the least blue.

the acyl chain restricts the chain to a well-specified position within the laminated β-sheets (Figure 6b,c). The resulting model for the *N*-lauroyl-KLVFFAE peptide–amphiphile assembly increases both the distance between adjacent β-sheets (Figure 6c) and the hydrophobicity of the solvent exposed tube surfaces (Figure 6d) relative to the *N*-acetyl capped peptide.

These data highlight a remarkable plasticity of the cross-β structural element as revealed in this unique and unexpected capacity of the cross-β fold to accommodate acyl chains within the interior of the β-sheet laminate. Although the structure models suggest that the C_{12} acyl chain does not

occupy the complete laminate surface, it is positioned to fill a well-defined cavity around these side chains. The shorter C_5 to C_{10} chain may only partially occupy this laminate cavity and therefore not assemble as a single thermodynamic assembly, whereas the longer C_{14} to C_{16} alkanes may assemble into multiple structures. Isotope-edited IR of [1-^{13}C]Phe19-enriched peptides (Supporting Information, Figure S9) indicate that the β-sheet registry for chain lengths from C_2 to C_{13} are identical with antiparallel out-of-register β-sheets, but that C_{14} and C_{16} Aβ(16-22) form parallel β-sheets. The parallel β-sheet registry would allow for peptide amphiphile conformations, as suggested in worm-like micelle and nanobelt models, where acyl chains are sequestered from solvent and charged head groups are exposed to solvent;[4–6,8,25] however, further solid-state NMR analysis is needed to localize the C_{14} and C_{16} acyl chains with respect to the peptide backbone.

A key difference between the *N*-lauroyl-Aβ(16-22) peptide amphiphile model (Figure 5c) and typical worm-like micelles is the antiparallel β-sheet registry and burial of half of the positively charged lysine sidechains, which are passivated by negatively charged TFA anions (Supporting Information, Figure S7) as previously observed[23] in the *N*-acetyl Aβ(16-22) bilayer structure. Remarkably however, the antiparallel β-sheet registry and the ability of these simple cross-β assemblies to expand in an accordion-like fashion (Figure 1b) to accommodate acyl chains between the stacks of β-sheets greatly extends the molecular geometries available to cross-β assemblies and introduces a radically new phase for the peptide amphiphiles that must now be considered in the structural models for all known assemblies.[2–4] The ability to systematically alter the spacing on these solvent accessible surfaces, ones already known to bind small molecules[18] and metal arrays,[27] by simply incorporating a saturated carbon chain within the cross-β laminate core will provide entirely new strategies for the creation of well-ordered mesoscale assemblies.[5,25,28] It has also not escaped our attention that other amyloid and prion proteins could well sequester lipids as they assemble, particularly those generated within biological membranes, providing further insight into the physiological data that implicates more complex aggregates as critical for disease symptoms.[29]

Experimental Section

Peptides were synthesized by standard solid-phase Fmoc (9-fluorenylmethyloxycarbonyl) chemistry.[10] N-termini of *N*-acyl-Aβ(16-22) were capped with standard coupling of the corresponding acyl acid with resin overnight. The ^{13}C{^{15}N} REDOR pulse sequence[22] consists of an *S* sequence with both ^{13}C and ^{15}N π pulses, and the S_0 sequence, which does not contain any ^{15}N pulses. The difference between the REDOR *S* and S_0 signal (ΔS) is directly proportional to the dipolar coupling, and thus the distance between the two spins.

Received: February 13, 2012
Revised: April 24, 2012

Keywords: amphiphiles · nanotubes · NMR spectroscopy · peptides · self-assembly

[1] A. Mueller, D. F. O'Brien, *Chem. Rev.* **2002**, *102*, 727–758.
[2] S. R. Bull, M. O. Guler, R. E. Bras, T. J. Meade, S. I. Stupp, *Nano Lett.* **2005**, *5*, 1–4.
[3] D. J. Gordon, J. J. Balbach, R. Tycko, S. C. Meredith, *Biophys. J.* **2004**, *86*, 428–434.
[4] J. D. Hartgerink, E. Beniash, S. I. Stupp, *Science* **2001**, *294*, 1684–1688.
[5] F. Versluis, H. R. Marsden, A. Kros, *Chem. Soc. Rev.* **2010**, *39*, 3434–3444.
[6] X. Zhao, F. Pan, H. Xu, M. Yaseen, H. Shan, C. A. Hauser, S. Zhang, J. R. Lu, *Chem. Soc. Rev.* **2010**, *39*, 3480–3498.
[7] R. C. Elgersma, T. Meijneke, R. de Jong, A. J. Brouwer, G. Posthuma, D. T. Rijkers, R. M. Liskamp, *Org. Biomol. Chem.* **2006**, *4*, 3587–3597.
[8] M. Deng, D. Yu, Y. Hou, Y. Wang, *J. Phys. Chem. B* **2009**, *113*, 8539–8544.
[9] J. J. Balbach, Y. Ishii, O. N. Antzutkin, R. D. Leapman, N. W. Rizzo, F. Dyda, J. Reed, R. Tycko, *Biochemistry* **2000**, *39*, 13748–13759.
[10] A. K. Mehta, K. Lu, W. S. Childers, Y. Liang, S. N. Dublin, J. Dong, J. P. Snyder, S. V. Pingali, P. Thiyagarajan, D. G. Lynn, *J. Am. Chem. Soc.* **2008**, *130*, 9829–9835.
[11] F. T. Senguen, N. R. Lee, X. Gu, D. M. Ryan, T. M. Doran, E. A. Anderson, B. L. Nilsson, *Mol. Biosyst.* **2011**, *7*, 486–496.
[12] S. A. Petty, S. M. Decatur, *J. Am. Chem. Soc.* **2005**, *127*, 13488–13489.
[13] H. Inouye, K. A. Gleason, D. Zhang, S. M. Decatur, D. A. Kirschner, *Proteins Struct. Funct. Bioinf.* **2010**, *78*, 2306–2321.
[14] M. Sunde, L. C. Serpell, M. Bartlam, P. E. Fraser, M. B. Pepys, C. C. F. Blake, *J. Mol. Biol.* **1997**, *273*, 729–739.
[15] P. Sikorski, E. D. Atkins, L. C. Serpell, *Structure* **2003**, *11*, 915–926.
[16] O. S. Makin, P. Sikorski, L. C. Serpell, *J. Appl. Crystallogr.* **2007**, *40*, 966–972.
[17] W. S. Childers, R. Ni, A. K. Mehta, D. G. Lynn, *Curr. Opin. Chem. Biol.* **2009**, *13*, 652–659.
[18] W. S. Childers, A. K. Mehta, K. Lu, D. G. Lynn, *J. Am. Chem. Soc.* **2009**, *131*, 10165–10172.
[19] K. Lu, V. P. Conticello, D. G. Lynn, *Mater. Res. Soc. Symp. Proc.* **2004**, *826*, 1–6.
[20] A. Barth, C. Zscherp, *Q. Rev. Biophys.* **2002**, *35*, 369–430.
[21] S. M. Decatur, *Acc. Chem. Res.* **2006**, *39*, 169–175.
[22] T. Gullion, J. Schaefer, *J. Magn. Reson.* **1989**, *81*, 196–200.
[23] W. S. Childers, A. K. Mehta, R. Ni, J. V. Taylor, D. G. Lynn, *Angew. Chem.* **2010**, *122*, 4198–4201; *Angew. Chem. Int. Ed.* **2010**, *49*, 4104–4107.
[24] J. D. Gehman, F. Separovic, K. Lu, A. K. Mehta, *J. Phys. Chem. B* **2007**, *111*, 7802–7811.
[25] I. W. Hamley, *Soft Matter* **2011**, *7*, 4122–4138.
[26] A. K. Ghose, V. N. Viswanadhan, J. J. Wendoloski, *J. Phys. Chem. A* **1998**, *102*, 3762–3772.
[27] J. Dong, J. M. Canfield, A. K. Mehta, J. E. Shokes, B. Tian, W. S. Childers, J. A. Simmons, Z. Mao, R. A. Scott, K. Warncke, et al., *Proc. Natl. Acad. Sci. USA* **2007**, *104*, 13313–13318.
[28] W. S. Childers, A. K. Mehta, T. Q. Bui, Y. Liang, D. G. Lynn, *Molecular Self-Assembly: Advances and Applications*, *1st ed.* (Ed.: A. Li), Pan Stanford Publishing, Singapore, **2012**.
[29] R. F. Rosen, L. C. Walker, H. Levine 3rd, *Neurobiol. Aging* **2011**, *32*, 223–234.

